Deformation-Mechanism Map for Nanocrystalline Metals by Molecular-Dynamics Simulation

Article *in* Nature Materials · February 2004

DOI: 10.1038/nmat1035 · Source: PubMed

5 authors, including:

V. Yamakov
Analytical Mechanics Associates
105 PUBLICATIONS **6,499** CITATIONS
SEE PROFILE

Simon Robert Phillpot
University of Florida
405 PUBLICATIONS **32,057** CITATIONS
SEE PROFILE

Amiya K. Mukherjee
University of California, Davis
509 PUBLICATIONS **20,301** CITATIONS
SEE PROFILE

H. Gleiter
Karlsruhe Institute of Technology
367 PUBLICATIONS **31,460** CITATIONS
SEE PROFILE

Deformation-mechanism map for nanocrystalline metals by molecular-dynamics simulation

V. YAMAKOV[1,†], D. WOLF*[1], S. R. PHILLPOT[1,‡], A. K. MUKHERJEE[2] AND H. GLEITER[3]

[1]Materials Science Division, Argonne National Laboratory, Argonne, Illinois 60439, USA
[2]Division of Materials Science & Engineering, Department of Chemical Engineering and Materials Science, University of California, Davis, California 95616, USA
[3]Institut für Nanotechnologie, Forschungszentrum Karlsruhe, 76021 Karlsruhe, Germany
[†]Present address: National Institute of Aerospace, Hampton, Virginia 23666, USA
[‡]Present address: Department of Materials Science and Engineering, University of Florida, Gainesville, Florida 32611, USA
*e-mail: wolf@anl.gov

Published online: 14 December 2003; doi:10.1038/nmat1035

Molecular-dynamics simulations have recently been used to elucidate the transition with decreasing grain size from a dislocation-based to a grain-boundary-based deformation mechanism in nanocrystalline f.c.c. metals. This transition in the deformation mechanism results in a maximum yield strength at a grain size (the 'strongest size') that depends strongly on the stacking-fault energy, the elastic properties of the metal, and the magnitude of the applied stress. Here, by exploring the role of the stacking-fault energy in this crossover, we elucidate how the size of the extended dislocations nucleated from the grain boundaries affects the mechanical behaviour. Building on the fundamental physics of deformation as exposed by these simulations, we propose a two-dimensional stress-grain size deformation-mechanism map for the mechanical behaviour of nanocrystalline f.c.c. metals at low temperature. The map captures this transition in both the deformation mechanism and the related mechanical behaviour with decreasing grain size, as well as its dependence on the stacking-fault energy, the elastic properties of the material, and the applied stress level.

The idea of representing the deformation behaviour of materials in a two-dimensional-map format was first put forward in 1965[1]. The basic principle of such representations is to use the best available constitutive equations[2,3] that describe the operative deformation mechanisms for dividing the deformation-parameter space into individual regions within which a single mechanism is rate controlling[4,5]. The deformation-parameter space usually consists of two of the three normalized parameters: stress σ/G, temperature, T/T_M, and grain size, d/b (here σ is stress, G is the shear modulus, T_M the melting temperature, d the grain size, and b the Burgers vector of the lattice dislocations). For example, the constitutive equation for elevated-temperature crystal plasticity[2], anticipates low-temperature superplasticity[6] and high strain-rate superplasticity[7,8]. Both phenomena have now been experimentally observed in nanocrystalline materials[9,10] (that is, polycrystals with a grain size of less than 100 nm). This success implies that the deformation-map technique can possibly be extended to nanocrystalline materials. However, such an extension is not straightforward because the mechanical behaviour of these materials is still controversial[11], the observations ranging from greatly enhanced ductility[12–15] to dramatically increased yield strength[16–19]. The prevalent deformation maps apparently cannot resolve this controversy, because they are based on empirical relations, rather than on fundamental physical principles.

Here we construct a deformation-mechanism map based on fundamental physical processes in the deformation of nanocrystalline f.c.c. metals. The knowledge for these processes comes from modelling the nanocrystalline microstructure at the atomic level by using molecular-dynamics (MD) simulation. This is in contrast to the prevalent approach, where the deformation maps are built on phenomenological constitutive equations, which result from assumptions on certain deformation mechanisms derived from empirical data. The power of our approach is that it integrates the most important physics associated with deformation phenomena, in a self-consistent description of the effects of stress and grain size on the strain rate in nanocrystalline structures, thereby avoiding the empiricism of

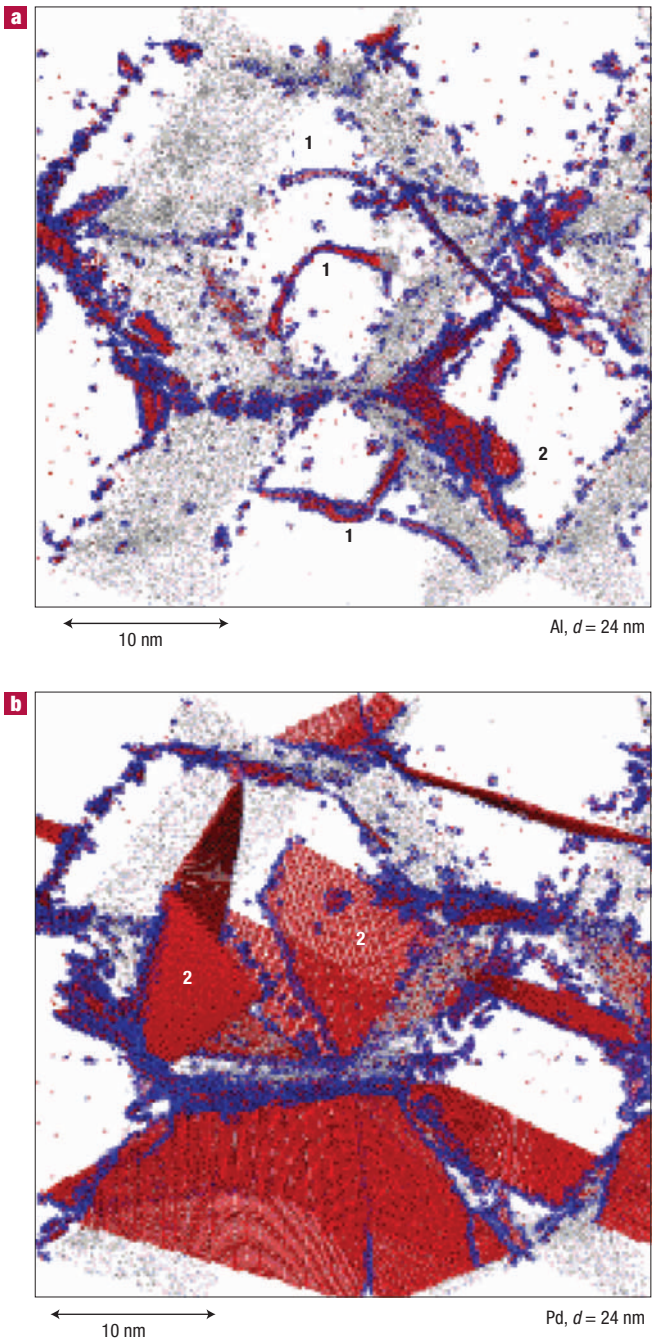

Figure 1 Comparison of two snapshots taken after 1% plastic straining of two identical microstructures of (a) a high- and (b) a low-SFE material with a grain size of 24 nm. To ensure similar deformation conditions, each system was loaded under uniform tensile stress approximately 0.1 GPa above its respective dislocation–nucleation threshold stress for this grain size. **a**, Al (with a SFE of 122 mJ m^{-2}) and **b**, a hypothetical low-SFE material, referred to as 'low-SFE Pd', with a SFE of 8 mJ m^{-2}. Two distinct types of dislocation configurations are labelled as (1), indicating a complete, extended 1/2[110] dislocation and (2), indicating a stacking-fault plane produced by a single Shockley-partial dislocation emitted from a GB.

the prevalent approach. Moreover, ultimately this approach can test the basic assumptions underlying the phenomenological equations, assess the possible relevance of previously proposed mechanisms, and be of use to discover new deformation mechanisms not yet suggested in the literature and incorporate them in the deformation maps.

Our deformation map is based on the physics of nucleation and propagation of dislocations in nanocrystalline f.c.c. metals at room temperature, as exposed by MD simulation. Simulations for idealized, fully three-dimensional (3D) nanocrystalline-Al microstructures with a grain size of up to 32 nm provided a detailed understanding of (i) the processes of dislocation nucleation and glide in the nanograins and (ii) the crossover with decreasing grain size in the deformation mechanism and in the related mechanical behaviour, from dislocation slip to a grain-boundary-based deformation process[20]. Building on these insights, here we use the same simulation model[20] to investigate the effect of the stacking-fault energy (SFE) on the deformation behaviour. Our comparison of a low-SFE f.c.c. metal with the behaviour of Al, a high-SFE metal, provides novel insights into the structure and dynamics of the nucleated dislocations and their effect on the 'strongest size'[19] at which the crossover from a dislocation to a grain boundary (GB)-based mechanism occurs. These atomic-level insights enable us to subsequently construct our deformation map.

Simulations of fully 3D nanocrystalline-Al microstructures[20] revealed the nucleation of complete 1/2[110] dislocations from the GBs and triple junctions, provided the grain size d is large enough ($d \geq 18$ nm). As in coarse-grained Al, these dislocations are dissociated into two 1/6[112] Shockley partials connected by a stacking fault; however, by contrast with a coarse-grained material or a single crystal, these loops terminate on the GBs rather than within the grains[20]. As d decreases below 18 nm, complete dislocations can no longer be nucleated, and only individual partials, travelling across the grains while leaving behind stacking faults transecting the grains, are observed. However, since the nucleation stress increases as $1/d$ (see below), under the constant-stress deformation eventually all dislocation nucleation ceases, and a GB process takes over. This is the 'inverse Hall–Petch' deformation regime to which, with commonly available computational resources, virtually all previous computer simulations of fully 3D nanocrystalline materials have been limited (see, for example, refs 21–23).

The crossover in the deformation mechanism arises from the length-scale competition between the grain size and the dislocation splitting distance, r. The latter depends on the resolved shear stress, σ, and the SFE, γ, via the relation[24]

$$r = \frac{r_0(\gamma)}{1-\sigma/\sigma_\infty(\gamma)} \quad , \qquad (1)$$

where $r_0 = K_1 b^2/\gamma$ is the equilibrium splitting distance at $\sigma = 0$; b is the Burgers vector of the Shockley partial dislocation, and $\sigma_\infty(\gamma) = K_2\gamma$ is the resolved shear stress at which the splitting distance becomes infinitely large. The constants K_1 and K_2 depend on the elastic moduli of the material and the particular types of the two Shockley partials[24].

An important aspect of the interplay between dislocation-dominated and GB-mediated deformation processes, characterized by the competition between the two length scales defined by r (see equation (1)) and d, can be demonstrated by comparing the deformation behaviour of a material with a high SFE, Al, with that of a hypothetical material with a low-SFE, which we name 'low-SFE Pd' (see Methods).

Two identical microstructures with a grain size of 24 nm of the two potentials representing low and high SFE materials were loaded under uniform tensile stress slightly higher than the dislocation-nucleation threshold stress for these potentials (see Methods). As shown in Fig. 1a and b, after 1% plastic straining, the difference in the SFE has produced very different dislocation patterns in the two systems. The Al system shown in Fig. 1a exhibits a series of loops of perfect dislocations propagating through the grain interiors. By contrast, in low-SFE Pd, complete dislocations could not be nucleated for this grain size and the grain interiors are transected

by a number of stacking-fault planes lying on several slip systems (see Fig. 1b).

The time-dependent plastic strains obtained for the two model materials after subtracting the corresponding elastic strains are compared in Fig. 2. Remarkably, although initially (that is, up to a strain of ~0.4%) the two materials behave quite similarly, for larger plastic strains the two systems evolve qualitatively rather differently. Following a steady-state deformation regime, after ~1% plastic strain, the strain rate in Al is approximately constant; by contrast, after a much smaller steady-state regime, the strain rate in the low-SFE material decreases steadily.

We interpret these distinct behaviours by observing that up to about 0.4% plastic strain, both systems nucleate only partial dislocations which propagate, with about equal velocity, into the grain interiors, giving rise to rather similar strain rates. (As the stress applied to each system, lying ~0.1 GPa above the respective nucleation-threshold stress, was chosen so as to create similar deformation conditions, these rather similar initial strain rates are to be expected.) At this point, the two curves in Fig. 2 start to diverge. The high-SFE material is then able to emit second partials to form complete, perfect dislocations (see Fig. 1a), thus entering the 'perfect dislocation slip' regime in Fig. 2. At the same time, in the low-SFE material, such closing partials cannot appear because, for equal stacking-fault lengths, the system energy has increased by much less than in the high-SFE material. Instead, the stacking faults continue to extend through glide of the single partials, eventually transecting the entire grain and, inevitably, blocking the propagation of any later-formed stacking faults (see Fig. 1b). The inability of the low-SFE metal to produce perfect dislocations consequently leads to the strain hardening seen in Fig. 2 (see the 'partial slip' regime).

This situation in which $d < r$ for the low-SFE metal is qualitatively identical to that of a high-SFE metal, but with a much smaller grain size. However, an important difference between the two materials arises from the strong, d^{-3}–d^{-2} grain-size dependence of the competing GB-based deformation process (namely GB-diffusion creep)[20,25]. Whereas in the high-SFE metal, the small grain size enables the GB-mediated deformation to dominate, the larger grain size in the low-SFE metal favours the partial dislocation slip.

By contrast with our previous simulations of dislocation processes in columnar microstructures[26,27], in which the dislocations were constrained to be straight lines, here the dislocation lines are curved and they terminate on the GBs[20]. Cheng *et al.*[28] suggested that this introduces a grain-size dependence into the nucleation threshold stress. They proposed the existence of a GB dislocation source of the Frank–Read type, with a characteristic size of the order of the average distance between the triple lines. Further, assuming an inverse proportionality between the loop radius and the stress acting on the loop, they suggested[28] that the size of the loops nucleated from the GBs is proportional to the grain size, that is, that the nucleation stress is inversely proportional to the grain size, $\sigma_n \sim 1/d$. When the grains become larger, of micrometre size, the mechanism changes to the one considered by Li[29] as nucleation of dislocations from GB ledges and their propagation through the forest dislocations commonly present in coarse-grained materials. This mechanism gives a Hall–Petch type of nucleation stress, $\sigma_n = \sigma_0 + k/\sqrt{d}$, where σ_0 is the single-crystal yield stress and k is a constant depending on the strength of the GB[29]. Combining the two mechanisms one gets:

$$\sigma_n = \sigma_0 + k/\sqrt{d} \quad \text{for coarse-grained metals} \qquad (2a)$$

$$\sigma_n \sim 1/d \quad \text{for nanocrystalline metals.} \qquad (2b)$$

These insights into the dislocation-nucleation mechanism and the structure of the dislocations in nanocrystalline f.c.c. metals can be captured in a deformation-mechanism map. The underlying physics comes from the length-scale competition between the grain size, d, and the splitting distance, r (see equation (1)), and from the grain-size dependence of the dislocation nucleation stress (see equation (2)). In this way, the map connects the mechanical properties of nanocrystalline f.c.c. metals with the structure and physics of the dislocations present in the deformation process. Based on equation (1), this map (presented in Fig. 3) is expressed in coordinates of reduced stress, σ/σ_∞, and reduced inverse grain size, r_0/d. r_0 and σ_∞ are therefore material-defining parameters, in contrast to the use of b and G, which normalize the variables d and σ in the phenomenological constitutive equations on which the prevalent deformation maps are built[1–5].

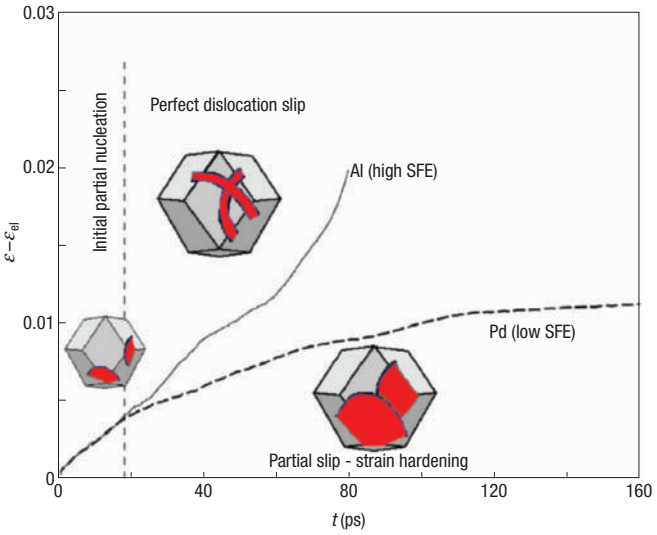

Figure 2 Comparison of the plastic strain versus time behaviour of a high- and low-SFE material for a grain size of 24 nm. The deformation conditions are as for Fig. 1. By contrast with the high-SFE material Al, the inability of low-SFE Pd to produce perfect dislocations leads to strain hardening. The plastic strain $\varepsilon_{pl} = \varepsilon - \varepsilon_{el}$ is obtained by subtracting the elastic strain, ε_{el}, from the total strain, ε.

The variables in this map (see Fig. 3) range within the natural limits $0 \le \sigma/\sigma_\infty \le 1$ and $0 \le r_0/d \le 1$. Whereas the line at $\sigma = \sigma_\infty$ defines the upper stress limit, the line at $d = r_0$ defines a lower grain-size limit of stability for the grains. At $\sigma = \sigma_\infty$, the stacking-fault splitting distance becomes infinite. This means that an entire (111) plane can shear in the [112] direction, and the crystal structure becomes mechanically unstable. The limit for $r_0/d = 1$ defines a grain size equal to the equilibrium stacking-fault splitting distance under zero applied load (see Fig. 3). This implies that grains of size less than r_0 would be unstable even at zero stress, and the structure would approach the amorphous limit. For the Al potential used here[30], $r_0 \approx 1$ nm (refs 26, 31), that is, a value of the order of the GB width.

Within these limits, the map is transected by two straight diagonal lines (Fig. 3). The 'dislocation-splitting line', $d = r$ (defined by equation (1)), represents all the points at which the splitting distance is equal to the grain size. The 'nucleation-stress' line is defined by equation (2). It represents the dividing line above which either complete or only partial dislocations are present. We note that σ_0 and $k/\sqrt{d}$ in equation (2a) are much smaller than σ_∞: for pure Al the fit to the Hall–Petch slope gives[32] $\sigma_0 = 5.91 \times 10^{-3}$ GPa and $k = 7.06 \times 10^{-5}$ m$^{1/2}$ GPa; by comparison, σ_∞ calculated for the case of a dislocation dissociated into a screw and an edge partial dislocations[24] gives a value of $\sigma_\infty \approx 1.5$ GPa. (It should be noted that this value is lower than the theoretical shear strength, $\sigma_r = 2.84$ GPa, calculated in ref. 33 under the assumption of multi-plane rather than single-plane shear.)

Because σ_0 and $k/\sqrt{d}$ in equation (2a) are much smaller than σ_∞, in practice the coarse-grained regime corresponding to equation (2a) will

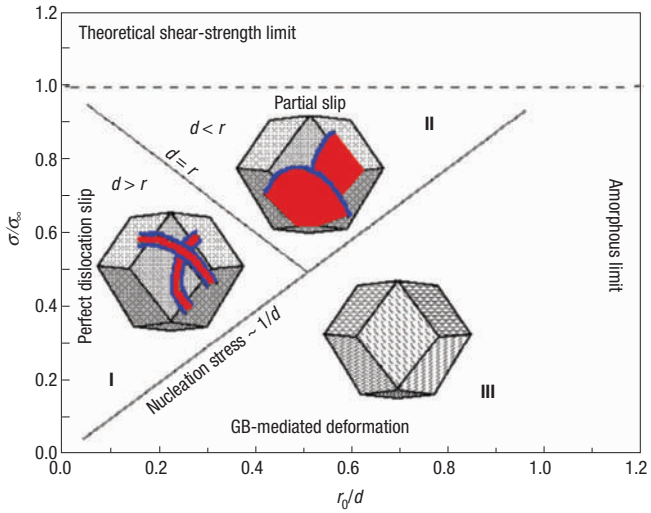

Figure 3 Proposed deformation-mechanism map incorporating the role of the stacking-fault energy in the deformation behaviour. The map shows three distinct regions in which either complete extended dislocations (Region I) or partial dislocations (Region II), or no dislocations at all (Region III) exist during the low-temperature deformation of nanocrystalline f.c.c. metals. The map is expressed in reduced units of stress (σ/σ_∞) and inverse grain size (r_0/d; see equation (1)). The parameters σ_∞ and r_0 are functions of the stacking-fault energy and the elastic properties of the material.

not show up on the scale of Fig. 3; only the nanocrystalline part, $\sigma_n \sim 1/d$, is therefore shown. As we were not able at this time to determine the slope of this line, it is reasonable to assume that at $d = r_0$, $\sigma_n = \sigma_\infty$; this then gives a slope of 1. As below this line no dislocations are present at all, the splitting line terminates at the nucleation line. The map is thus divided into three regions.

In Region I, characteristic of a large grain size and/or a high-SFE metal, slip deformation prevails as the grains are larger than r and complete, extended dislocations nucleated from the GBs can propagate across the grains. We note that when $r/d \to 0$, one should use equation (2a) (not shown in Fig. 3).

In Region II, characteristic of a small grain size and/or a low-SFE metal, only incomplete dislocations can be nucleated; the grains are therefore transected by stacking faults that inhibit dislocation propagation, thus giving rise to strain hardening. The transition from Region I to Region II at the splitting line ($d = r$) marks the transition from conventional to partial slip. This line also naturally connects the two points of crystal instability, $\sigma = \sigma_\infty$ with $d = r_0$, as discussed above.

Region III characterizes the very small grain-size or low-stress regime in which no dislocations are present at any stress, and the deformation is therefore controlled by GB-mediated processes. These processes involve GB diffusion creep, that is, coupled GB sliding[21–23] and GB diffusion[25], resulting in the inverse Hall–Petch behaviour of the nanocrystalline metal[20,34].

According to this map, the 'strongest size' may arise from two different scenarios for high and low SFE or at low and high stress. For high-SFE metals, Region II involves very high stress and the crossover from normal to inverse Hall–Petch behaviour should be governed mainly by the transition from perfect slip to GB-mediated deformation[20], that is, the $1/d$ line between Region I and III; for low-SFE metals or high stress, the process involves partial slip in Region II as an intermediate stage. As long as the grains are smaller than r, they would always be transected by stacking faults, and their size should not influence the resulting strain hardening. Meanwhile, GB processes increase rapidly with decreasing grain size, leading to softening. Thus we expect that the 'strongest size' in this case is at the line $d = r$ and increases with decreasing SFE[26].

Although the above map represents an attempt to extrapolate the atomic mechanisms observed in MD simulations to a deformation regime that is accessible experimentally and in real materials, it is important to be aware of the inherent limitations of the MD approach. Apart from being restricted to relatively small model systems, by their very nature, MD simulations are limited to very high stresses and, hence, strain rates (of typically $>10^7$ s^{-1}, corresponding to 1% strain in 1 ns). The stresses applied in the present simulations, although high, are not entirely unusual in experimental studies of nanocrystalline materials. In fact, experiments[5] on nanocrystalline Ni_3Al show dislocation nucleation and propagation for a grain size of 50 nm at a stress of 1.5 GPa, that is, very similar to our simulation conditions. The transition from partial to perfect slip in nanocrystalline Al has also been observed experimentally[35]. The issue of the high strain rates in MD simulations was recently also addressed in high-temperature deformation simulations[25] of nanocrystalline Pd. In spite of the extremely high strain rates (of $>10^7$ s^{-1}), these simulations quantitatively validated the Coble-creep equation[36] describing GB diffusion creep in coarse-grained materials. However, as discussed in detail in ref. 34, special care must be taken in low-temperature simulations to ensure that a process that might otherwise dominate the deformation behaviour (that is, under experimental observation conditions) is not inadvertently suppressed, and hence overlooked, during the short time window to which MD simulations are inherently limited.

In summary, our study reveals how the crossover with decreasing grain size from dislocation-driven to GB-mediated deformation depends on the stacking-fault energy, the elastic properties of the material, and the magnitude of the applied stress. These insights suggest a novel deformation-mechanism map for nanocrystalline f.c.c. metals, which captures this crossover in both the prevailing deformation mechanism and the mechanical behaviour. This map provides a bridge between the fundamental physics of plastic deformation as exposed by MD simulation, and experiments towards deconvoluting the deformation behaviour of nanocrystalline materials.

METHODS

Our simulations were performed on idealized, fully dense and impurity-free model microstructures consisting of four grains of identical size and shape in the periodically repeated simulation cell. These input structures were prepared using a Voronoi construction with the grain centres placed on a 3D periodic f.c.c. lattice. The resulting grains have the shape of the f.c.c. Wigner–Seitz cell—a rhombic dodecahedron with 12 faces. By choosing random grain orientations and applying a Monte-Carlo procedure to avoid low-angle, vicinal and 'special' high-angle misorientations, we ensure that all the GBs in the system are general, high-energy GBs with a highly disordered atomic structure. Owing to the large number of faces per grain (12), the system forms a rather large number of GBs per unit volume (for a total of 24 distinct GBs in the simulation cell). The GBs meet at the triple lines at 120° angles, that is, close to the equilibrium angles; this ensures a high degree of stability against grain growth.

Two interatomic potentials representing low and high SFE metals were applied. As representative for a low-SFE metal we consider a hypothetical material, which we name 'low-SFE Pd', described[37] by the EAM potential for Pd. This potential was fitted to bulk properties of Pd and yields a very low SFE of 8 mJ m^{-2}, compared with the experimental value[38] of ~180 mJ m^{-2}. By contrast, with a SFE of 122 mJ m^{-2}, the Ercolessi and Adams potential[30] for Al is representative for a high-SFE metal.

We use the Parrinello–Rahman constant-load technique[39] combined with the Nose–Hoover thermostat[40] to achieve constant stress–constant temperature dynamics. All of our MD simulations were carried out at temperature $T = 300$ K. Constant tensile loads of 2.0 GPa for Al and 1.5 GPa for Pd, slightly higher than the dislocation-nucleation threshold stress of the two potentials (defined as the stress at which GBs start to nucleate partial dislocations and determined to be 1.4 GPa for low-SFE Pd and 1.8–1.9 GPa for Al for the 24-nm grain size) were applied along one of the main axes of the simulation cell. This gives a maximum resolved shear stress on the glide planes below 1 GPa for Al and below 750 MPa for Pd, that is, well below the theoretical shear strengths of these materials. (For example, the theoretical shear strength for Al at $T = 0$ K has been calculated[33] to be 2.84 GPa.)

Throughout our simulations we use common-neighbour analysis (CNA)[41] to identify the stacking faults in our microstructures as double layers of atoms in h.c.p. surroundings. Atoms that are neither in perfect f.c.c. nor h.c.p. surroundings as defined by CNA are 'disordered atoms'; these are useful to identify the GBs and the dislocation cores. In the simulation snapshots shown in this paper, we use the following convention. Atoms in perfect f.c.c. surrounding are not shown; all atoms in h.c.p. surroundings are visualized in red; atoms that have more than a third of their neighbours (including first and second nearest neighbours) as disordered atoms are considered to be in a highly disordered environment and are visualized in blue.

To best expose all the dislocation processes inside the grains while still keeping track of the grains themselves, we chose to visualize only a small part of each GB. This part is chosen with respect to a line of observation along one of the diagonals of the simulation cell. The GBs are then visualized as walls of grey atoms. (For more details, see ref. 20.)

Received 28 July 2003; accepted 10 November 2003; published 14 December 2003.

References

1. Weertman, J. & Weertman, J. R. in *Physical Metallurgy* (ed. Cahn, J. W.) 921–1010 (North-Holland, Amsterdam, 1965).
2. Mukherjee, A. K., Bird, J. E. & Dorn, J. F. Experimental correlations for high-temperature creep. *Trans. Am. Soc. Metals* **62,** 155–179 (1969).
3. Ashby, M. F. A first report on deformation-mechanism maps. *Acta Metall.* **20,** 887–897 (1972).
4. Frost, H. J. & Ashby, M. F. *Deformation-Mechanism Maps: The Plasticity and Creep of Metals and Ceramics* (Pergamon, Oxford, 1982).
5. Mukherjee, A. K. An examination of the constitutive equation for elevated temperature plasticity. *Mat. Sci. Eng. A* **322,** 1–22 (2002).
6. McFadden, S. X., Mishra, R. S., Valiev, R. Z., Zhilyaev, A. P. & Mukherjee, A. K. Low-temperature superplasticity in nanostructured nickel and metal alloys. *Nature* **398,** 684–686 (1999).
7. Mukherjee, A. K., Mishra, R. S. & Bieler, T. R. Some critical aspects of high strain rate superplasticity. *Mater. Sci. Forum* **233–234,** 217–234 (1997).
8. Higashi, K. & Mabuchi, M. Recent works in high strain rate superplasticity. *Mater. Sci. Forum* **233–234,** 155 (1997).
9. Mishra, R. S., Valiev, R. Z., McFadden, S. X., & Mukherjee, A. K. Tensile superplasticity in a nanocrystalline nickel aluminide. *Mater. Sci. Eng.* **252,** 174–178 (1998).
10. Mishra, R. S., McFadden, S. X., Valiev, R. Z. & Mukherjee, A. K. Deformation mechanisms and tensile superplasticity in nanocrystalline materials. *J. Mater. Min. Soc.* **51,** 37–40 (1999).
11. Koch, C. C. & Suryanarayana, C. in *Microstructure and Properties of Materials* Vol. 2 (ed. Li, J. C. M.) 380–385 (World Scientific, Singapore, 2000).
12. Karch, J., Birringer, R. & Gleiter, H. Ceramics ductile at low-temperature. *Nature* **330,** 556–558 (1987).
13. McFadden, S. X., Mishra, R. S., Valiev, R. Z., Zhilyaev, A. P. & Mukherjee, A. K. Low-temperature superplasticity in nanostructured nickel and metal alloys. *Nature* **398,** 684–686 (1999).
14. Lu, L., Sui, M. L. & Lu, K. Superplastic extensibility of nanocrystalline copper at room temperature. *Science* **287,** 1463–1466 (2000).
15. Kim, B. N., Hiraga, K., Morita, K. & Sakka, Y. A high-strain-rate superplastic ceramic. *Nature* **413,** 288–291 (2001).
16. Nieh, T. G. & Wadsworth, J. Hall-Petch relation in nanocrystalline solids. *Scripta Met. Mater.* **25,** 955–958 (1991).
17. Siegel, R. W. Mechanical properties of nanophase materials. *Mater. Sci. Forum* **235–238,** 851–860 (1997).
18. Morris, D. G. & Morris, M. A., Hardness, strength, ductility and toughness of nanocrystalline materials. *Mater. Sci. Forum* **235–238,** 861–872 (1997).
19. Yip, S. Nanocrystals – the strongest size. *Nature* **391,** 532–533 (1998).
20. Yamakov, V., Wolf, D., Phillpot, S. R., Mukherjee, A. K. & Gleiter, H. Crossover in Hall–Petch behaviour in nanocrystalline materials by molecular-dynamics simulation. *Phil. Mag. Lett.* **83,** 385–393 (2003).
21. Schiotz, J., DiTolla, F. D. & Jacobsen, K. W. Softening of nanocrystalline metals at very small grain sizes. *Nature* **391,** 561–563 (1998).
22. Swygenhoven, H. V., Spaczer, M., Caro, A. & Farkas, D. Competing plastic deformation mechanisms in nanophase metals. *Phys. Rev. B* **60,** 22–25 (1999).
23. Swygenhoven, H. V., Derlet, P. M. & Hasnaoui, A. Atomic mechanism for dislocation emission from nanosized grain boundaries. *Phys. Rev. B* **66,** 024101 (2002).
24. Hirth, J. P. & Lothe, J. *Theory of Dislocations* 1st edn 306–353 (Wiley, New York, 1982).
25. Yamakov, V., Wolf, D., Phillpot S. R. & Gleiter, H. Grain-boundary diffusion creep in nanocrystalline palladium by molecular-dynamics simulation. *Acta Mater.* **50,** 61–73 (2002).
26. Yamakov, V., Wolf, D., Salazar, M., Phillpot S. R. & Gleiter, H. Length-scale effects in the nucleation of extended lattice dislocations in nanocrystalline Al by molecular-dynamics simulation. *Acta Mater.* **49,** 2713–2722 (2001).
27. Yamakov V., Wolf D., Phillpot S. R., Mukherjee A. K. & Gleiter H. Dislocation processes in the deformation of nanocrystalline aluminium by molecular-dynamics simulation. *Nature Mater.* **1,** 45–48 (2002).
28. Cheng, S., Spencer, J. A. & Milligan, W. W. Strength and tension/compression asymmetry in nanocrystalline and ultrafine-grain metals. *Acta Mater.* **51,** 4505–4518 (2003).
29. Li, J. C. M., Petch relation and grain boundary sources. *Trans. Metall. Soc. AIME* **227,** 239–247 (1963).
30. Ercolessi, F. & Adams J. B. Interatomic potentials from 1st-principle calculations – the force-matching method. *Europhys. Lett.* **26,** 583–588 (1994).
31. Bulatov, V. V., Richmond, O. & Glazo, M. V. An atomistic dislocation mechanism of pressure-dependent plastic flow in aluminum. *Acta Mater.* **47,** 3507–3514 (1999).
32. Mukai, T. & Higashi, K. Ductility enhancement of ultra fine-grained aluminium under dynamic loading. *Scripta Mater* **44,** 1493–1496 (2001).
33. Ogata, S., Li, J. & Yip, S. Ideal pure shear strength of aluminum and copper. *Science* **298,** 807–811 (2002).
34. Wolf, D., Yamakov, V., Phillpot, S. R. & Mukherjee A. K., Deformation mechanism and inverse Hall-Petch behaviour in nanocrystalline materials. *Z. Metallkd* **94,** 1091–1097 (2003).
35. Liao, X. Z. *et al.* A new deformation mechanism in nanocrystalline Al: partial dislocation slip. *Appl. Phys. Lett.* **83,** 632–634 (2003).
36. Coble, R. L. A model for boundary diffusion controlled creep in polycrystalline materials. *J. Appl. Phys.* **34,** 1679–1682 (1963).
37. Foiles, S. M. & Adams, J. B. Thermodynamic properties of fcc transition metals as calculated with the embedded-atom method. *Phys. Rev. B* **40,** 5909–5915 (1989).
38. Dillamore, I. L. & Smallman, R. E. The stacking-fault energy of f.c.c. metals. *Phil. Mag.* **12,** 191–193 (1965).
39. Parrinello, M. & Rahman, A. Polymorphic transitions in single crystals: A new molecular dynamics method. *J. Appl. Phys.* **52,** 7182–7190 (1981).
40. Melchionna, S., Ciccotti, G. & Holian, B. L. Hoover NPT dynamics for systems varying in shape and size. *Mol. Phys.* **78,** 533–544 (1993).
41. Clarke, A. S. & Jonsson, H. Structural changes accompanying densification of random hard-sphere packings. *Phys. Rev. E* **47,** 3975–3984 (1993).

Acknowledgements

V.Y., D.W. and S.R.P. are supported by the US Department of Energy, BES-Materials Science under contract W-31-109-Eng-38. V.Y. is also grateful for support from the DOE/BES Computational Materials Science Network (CMSN). A.K.M. acknowledges support from NSF-DMR. We are grateful for grants of computer time on the Cray-T3E at the John-von-Neumann-Institute for Computing in Jülich, Germany, and on the Chiba City Linux cluster at Argonne National Laboratory.
Correspondence and requests for materials should be addressed to D.W.

Competing financial interests

The authors declare that they have no competing financial interests.